Enhanced synaptic connectivity and epilepsy in C1q knockout mice

Yunxiang Chu[a,1,2], Xiaoming Jin[a,1,3], Isabel Parada[a], Alexei Pesic[a], Beth Stevens[b,4], Ben Barres[b], and David A. Prince[a,5]

[a]Departments of Neurology and Neurological Sciences and [b]Neurobiology, Stanford University School of Medicine, Stanford University, Stanford, CA 94305

Edited* by Edward G. Jones, University of California, Davis, CA, and approved March 12, 2010 (received for review December 12, 2009)

Excessive CNS synapses are eliminated during development to establish mature patterns of neuronal connectivity. A complement cascade protein, C1q, is involved in this process. Mice deficient in C1q fail to refine retinogeniculate connections resulting in excessive retinal innervation of lateral geniculate neurons. We hypothesized that C1q knockout (KO) mice would exhibit defects in neocortical synapse elimination resulting in enhanced excitatory synaptic connectivity and epileptiform activity. We recorded spontaneous and evoked field potential activity in neocortical slices and obtained video-EEG recordings from implanted C1q KO and wild-type (WT) mice. We also used laser scanning photostimulation of caged glutamate and whole cell recordings to map excitatory and inhibitory synaptic connectivity. Spontaneous and evoked epileptiform field potentials occurred at multiple sites in neocortical slices from C1q KO, but not WT mice. Laser mapping experiments in C1q KO slices showed that the proportion of glutamate uncaging sites from which excitatory postsynaptic currents (EPSCs) could be evoked ("hotspot ratio") increased significantly in layer IV and layer V, although EPSC amplitudes were unaltered. Density of axonal boutons was significantly increased in layer V pyramidal neurons of C1q KO mice. Implanted KO mice had frequent behavioral seizures consisting of behavioral arrest associated with bihemispheric spikes and slow wave activity lasting from 5 to 30 s. Results indicate that epileptogenesis in C1q KO mice is related to a genetically determined failure to prune excessive excitatory synapses during development.

complement cascade | seizure | synaptic pruning | development | axonal boutons

Early brain development is marked by an exuberant outgrowth of axons that innervate multiple targets. These projections are later refined through axonal pruning, a developmental regulatory process by which excessive connectivity is eliminated and mature patterns of neuronal innervation become established (1). Cortical synaptic pruning events, such as selective branch elimination for segregating layer V cortical neuronal projections to subcortical targets (1), and refinement of interhemispheric (2) and intracortical (3) are important for the development of precisely wired connections and normal information processing. The activation of a number of genes and proteins is crucial for the process of synaptic pruning in the mammalian brain (4). Recently, molecules ordinarily associated with immune and inflammatory processes have been shown to play nonimmune roles in synaptic pruning (5). C1q and C3 genes of the classical complement cascade are necessary for synapse elimination in the retino-geniculate pathway during development (6). Activation of C1q protein by astrocytes leads to triggering of a protease cascade, deposition of C3 and opsonization or "tagging" of synapses that are likely eliminated by microglia. Lateral geniculate relay neurons in C1q knockout (KO) mice deficient in these proteins retain multiple synaptic contacts from retinal ganglion cells that are normally eliminated during development (6).

C1q is also transiently expressed in synaptic regions of developing neocortex, particularly between postnatal day (P)4 and P10 (6), so that its absence in C1q KO mice might result in inadequate pruning and a "hyper-wired" cerebral cortex, i.e., one in which the enhanced circuitry present early in development would persist into adulthood. Increased recurrent excitation in complex neuronal networks of the neocortex (7) and hippocampus (8), due to sprouting of axons of excitatory glutamatergic neurons and formation of new functional connectivity after injury, can lead to excessive hypersynchronous discharges in large assemblies of neurons that underlie epileptogenesis (9). This acquired enhanced connectivity is, in some ways, a recapitulation of the situation early in brain development when excessive and mistargeted connections are present. We performed experiments in C1q KO and wild-type (WT) mice to test the hypothesis that defective neocortical pruning in KO animals might result in epilepsy. Results show that spontaneous and evoked epileptiform activity and increased intracortical excitatory connectivity are present in neocortical slices from C1q KO, but not WT mice. Video-EEG recordings from chronically implanted KO animals confirm that frequent behavioral seizures are occurring. The C1q KO mouse provides a remarkable example of spontaneous epileptogenesis due to a genetically determined developmental failure to prune.

Results

C1q KO Neocortical Slices Generate Epileptiform Activity. We initially recorded both spontaneous and evoked field potentials from layer V of in vitro sensorimotor cortical slices. In both WT and KO mice, short latency field potentials were evoked at threshold (Fig. 1*A 1* and *2*). In at least 1 slice from 9 of 10 C1q KO mice (21 of 31 slices), but 0 of 23 slices from WT mice, epileptiform activity was evoked by stimuli that were threshold or just above threshold for the initial response. Abnormal discharges consisted of all-or-none polyphasic events of variable form and latency lasting 150–400 ms, associated with bursts of action potentials (Fig. 1*A2*; see also Fig. 1*A4* and 1*B*, arrows). Evoked activity was blocked by more intense stimuli that were two or more times threshold (Fig. 1*A3*), as reported in other in vitro models of chronic epileptogenesis (10). In addition, spontaneous epileptiform events that had polyphasic morphology and durations similar to the evoked epileptiform potentials were recorded from cortical layer V in 17 of 23 slices from 6 of 7 C1q KO animals (Fig. 1*B*), but none of the 23 slices from WT mice. To determine whether epileptiform activity was focal or more generalized throughout a given slice, in 14 slices a pair of electrodes separated by ≈1mm was used to record spontaneous epileptiform activity in layer V at various distances from the midline (Fig. 1*C*). Spontaneous events could be recorded at

Author contributions: Y.C., X.J., and D.A.P. designed research; Y.C., X.J., I.P., and A.P. performed research; B.S. and B.B. contributed new reagents/analytic tools; Y.C., X.J., I.P., and A.P. analyzed data; and Y.C., X.J., and D.A.P. wrote the paper.

The authors declare no conflict of interest.

*This Direct Submission article had a prearranged editor.

[1]Y.C. and X.J. contributed equally to this work.

[2]Present address: Harvard-MIT Health Sciences and Technology, 77 Massachusetts Avenue, E25-519, Cambridge, MA 02139.

[3]Present address: Spinal Cord and Brain Injury Research Group, Department of Anatomy and Cell Biology and Stark Neurosciences Research Institute, Indiana University School of Medicine, Indianapolis, IN 46202.

[4]Present address: F.M. Kirby Neurobiology Center, Children's Hospital Boston, 300 Longwood Avenue CLS 12258 Boston, MA 02115.

[5]To whom correspondence should be addressed. E-mail: daprince@stanford.edu.

This article contains supporting information online at www.pnas.org/cgi/content/full/0913449107/DCSupplemental.

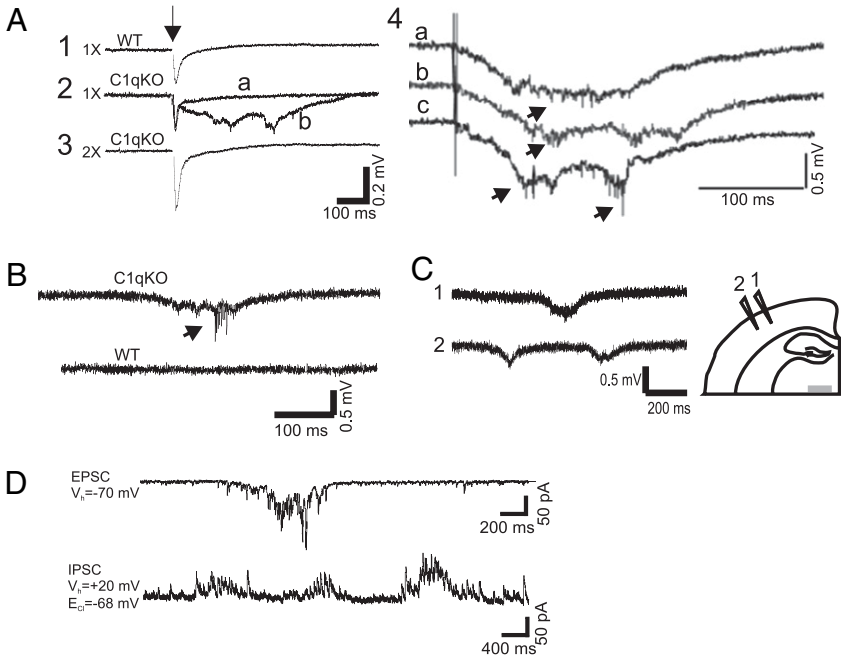

Fig. 1. Spontaneous and evoked epileptiform field potentials in cortical layer V of C1q KO brain slices. (*A*) Representative responses from P14 wild-type (WT) and C1q knockout (KO) animals to layer VI/white matter stimuli. (*A1*) Threshold stimulation (1×) evokes a short latency biphasic field potential in WT slice. (*A2*) Superimposed sweeps from a C1q KO slice show two consecutive responses to identical stimuli (0.2 Hz) that evoke either a short latency field potential, or a long duration, polyphasic all-or-none event. (*A3*) Epileptiform responses were blocked by increasing stimulus intensity to 2× threshold in slice of *A2*. Arrow marks time of stimulus. (*A4*) Additional examples of evoked epileptiform field potentials in slice from different C1q KO mouse. Arrows, action potentials (APs). (*B*) Spontaneous polyphasic epileptiform event with superimposed AP burst (arrow) from a P30 C1q KO brain slice (upper trace). Lower trace shows spontaneous activity from an age-matched, same-sex WT brain slice recorded simultaneously in the same chamber. (*C*) Spontaneous epileptiform activity from two electrodes spaced ≈1 mm apart in layer V of C1q KO cortical slice. Diagram shows position of the two recording electrodes. (*D*) Whole cell voltage clamp recording of bursts of spontaneous EPSCs (upper trace) and IPSCs (lower trace) from a C1q KO layer V pyramidal neuron. When the holding potential (V_h) is −70 mV, a burst of spontaneous inward polyphasic excitatory currents occurs lasting ≈800 ms. When V_h is +20 mV, bursts of spontaneous outward polyphasic inhibitory epileptiform currents are seen in the same neuron. (Scale bar: *C*, 1 mm.)

multiple sites, with significant latency in onset between electrodes. Analysis of laminar localization and spread of epileptiform events will require multielectrode recordings, however, present results suggest that epileptiform activity is widespread in cortex. Whole cell recordings (Fig. 1*D*) showed that spontaneous prolonged bursts of polysynaptic EPSCs and IPSCs, similar to those seen in other models of epileptogenesis in vitro (9), occurred in layer V pyramidal cells. Results show that C1q KO neocortical slices generate frequent epileptiform activity.

C1q KO Pyramidal Neurons Have Increased Excitatory Inputs. One explanation for the above hyperexcitability and epileptiform field potentials would be failure to prune excessive excitatory synapses, such as has been shown in geniculocortical relay cells of C1q KO mice of developing neocortex (6). Such enhanced excitatory innervation has been shown in other models of epileptogenesis in hippocampus and neocortex (9). To test this hypothesis, we mapped monosynaptic EPSCs onto 21 cortical layer V pyramidal neurons in the WT and 18 in KO mice by using whole cell recordings together with laser scanning photostimulation of slices perfused with ACSF-containing caged glutamate (11).

We first assessed possible changes in direct excitation of layer V pyramidal cells by glutamate in C1q KO mice by recording action potential (AP) firing evoked by glutamate uncaging in a cortical area of ≈400 × ≈600 μm around the somata of the recorded cells. The average maps of action potential number evoked by direct glutamate-induced depolarizations were similar between the WT and KO mice (Fig. S1 *A* and *B*). There were no significant differences in hotspot and spike number in circular areas at different distances from somata between the two groups (Fig. S1 *C* and *D*). The results indicated that neurons in WT and KO groups responded similarly to photostimulation in terms of direct excitability, with a spatial resolution of <150 μm.

Results of laser stimulation in layer V pyramidal neurons of WT sensorimotor cortex showed that most evoked EPSCs onto layer V pyramidal neurons originated from layer V in a region within 150~200 μm of the soma; contributions from other cortical laminae were much smaller (Fig. 2*A*). EPSC maps were significantly larger in C1q KO mice (Fig. 2*B*), with the C1q KO group having 25.9% more hotspots per map than the control group (28 ± 3% and 35 ± 3% hotspots per map for control and C1q group, respectively; $P < 0.05$, Student's t test). The hotspot ratio was also significantly larger in the KO than in the WT group (Fig. 2*D*, 0.28 ± 0.01 and 0.35 ± 0.01 for WT and KO, respectively; $P < 0.0001$, two-way ANOVA). The increases in hotspot ratio were present in both superficial and deep cortical layers in areas 100 μm and 350 μm below the somata ($P < 0.05$, Student's t test), and 250 μm and 500 μm superficial to the somata in layer V (Fig. 2*D*; $P < 0.05$ and $P < 0.005$, Student's t test). In contrast, the region normalized evoked EPSC amplitude, calculated by dividing the total amplitude of evoked events in a stimulus row by total number of spots in that row, was not significantly different between the two groups (Fig. 2*C*). The hotspot amplitude, calculated by dividing the total amplitude of evoked events in a stimulus row by total number of hotspots in that row, was also not significantly different in KO vs. control. These data suggest that layer V pyramidal neurons in the KO cortex are functionally connected to a greater number of presynaptic excitatory neurons in different layers of the cortex, whereas the strength of connectivity (i.e., amplitude of evoked EPSCs) was not enhanced.

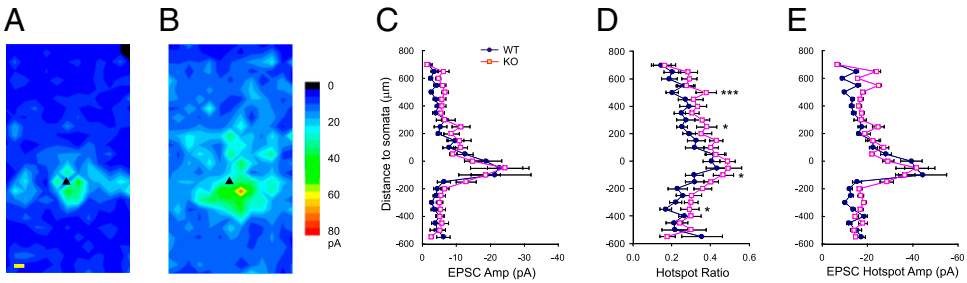

Fig. 2. Excitatory maps to layer V pyramidal neurons in the neocortex of C1q KO mice. (*A* and *B*) Average maps of excitatory synaptic connectivity to layer V pyramidal neurons in WT (*A*) and KO (*B*) mice. Note that the map in *B* is expanded significantly (see text). Black triangles, somata of the recorded layer V pyramidal neurons. Pial surface is above the top of map; white matter is on bottom. (*C*) Region normalized evoked EPSC amplitude, calculated by dividing the total amplitude of evoked events in a stimulus row by total number of spots in that row. (*D*) Hotspot ratio. (*E*) Hotspot EPSC amplitude in each row of maps, plotted at different cortical depths relative to the somata (at 0 μm) of layer V pyramidal neurons. (Scale bars: 50 μm). *, $P < 0.05$; **, $P < 0.01$; ***, $P < 0.005$.

As another index of functional connectivity, we recorded spontaneous EPSCs (sEPSCs) at the beginning of each mapping experiment, and miniature EPSCs (mEPSCs) from neurons in ACSF containing 1 μM tetrodotoxin after mapping. The frequencies of sEPSCs (representative traces in Fig. S2*A*) and mEPSCs (Fig. S2*B*) in layer V pyramidal cells of the KO group were significantly higher than in WT. The higher sEPSC and mEPSC frequencies in the KO group are consistent with the expanded excitatory input map and support the conclusion that more excitatory synapses are present on layer V pyramidal neurons. Interestingly, the lack of increase in the amplitude of EPSCs suggests that individual pyramidal cells do not hyper-innervate a given postsynaptic neuron, but rather contact more postsynaptic targets (7).

No Significant Change in Inhibitory Connectivity to Layer V Pyramidal Neurons. It is not known whether defective pruning and synapse elimination also affects axons of cortical interneurons in C1q KO mice. Using laser scanning photostimulation as above, we mapped inhibitory postsynaptic currents (IPSCs) onto the above group of layer V pyramidal neurons by changing the holding potential to +20 mV to reveal evoked IPSCs and minimize EPSCs. Uncaging stimuli evoked IPSCs as outward currents that had a large variability in amplitude. In IPSC maps of WT animals, most events were evoked in a circular area around somata, within a radius of ≈150 μm in layer V (Fig. S1*E*). In neurons of KO mice, the maps became slightly more defuse, with the appearance of more hotspots in the more superficial and deeper layers of the cortex (Fig. S1*F*). However, there were no significant differences in the number of hotspots per map, or in either the region normalized IPSC amplitude or hotspot ratio between the two groups (Fig. S1 *G* and *H*). There were also no significant differences in frequency of sIPSCs or mIPSCs between WT and C1q KO mice (Fig. S2 *D*–*F*). Results suggest that C1q differentially prunes excitatory vs. inhibitory connectivity during neocortical development.

Axonal Bouton Density Is Increased in C1q KO Pyramidal Neurons. We expected that failure to prune axons of pyramidal cells would be accompanied by an increased density of axonal boutons in C1q vs. WT mice. In the course of the whole cell recordings, 18 layer V pyramidal cells from 6 WT and 15 from 8 C1q KO mice (ages P27–31) were filled with biocytin (Fig. 3 *A* and *B*) and confocal images of comparable segments of their axons examined (*Materials and Methods*). Representative images from WT and mutant mouse axonal branches are shown in Fig. 3 *C* and *D*. A total of 1,665 μm of axonal length in secondary and tertiary branches was analyzed in WT and 2,169 μm in C1q KO mice. The mean interbouton distance was 3.73 ± 0.64 μm in 15 pyramidal cell axons from 8 C1q KO compared with 4.76 ± 0.60 μm in 18 axons from 6 WT mice (21.6% decrease, $P < 0.002$). These results are compatible with the conclusion that axonal bouton density is increased and that single layer V pyramidal cells of C1q KOs make more synapses. Taken together, these data and the laser mapping results indicate that there are pruning defects affecting excitatory synapses in the cortex of C1q KO mice. There was also a significant decrease in bouton size in C1q KO vs. WT axons (Fig. 3 *C* and *D* and Fig. S3). The ratio of small (≤1 μm diameter, small arrows; Fig. 3*D*) vs. large boutons (>1 μm, large arrows; Fig. 3*D*) in the axons of C1q KO pyramidal cells compared with those in WT neurons was 3.79 ± 1.19 for C1q KO cells and 0.57 ± 0.03 for WT cells, $P = 0.036$, Student's *t* test; Fig. S3). We speculate that this could be a consequence of failure to prune immature synapses (6).

C1q KO Mice Have Spontaneous Atypical Absence Seizures. The occurrence of spontaneous and evoked epileptiform discharges in in vitro neocortical slices from C1q KO mice raised the possibility that these animals might also have spontaneous seizures in vivo. Although we did not see any obvious convulsive activity during initial casual observations, the possibility that more subtle attacks

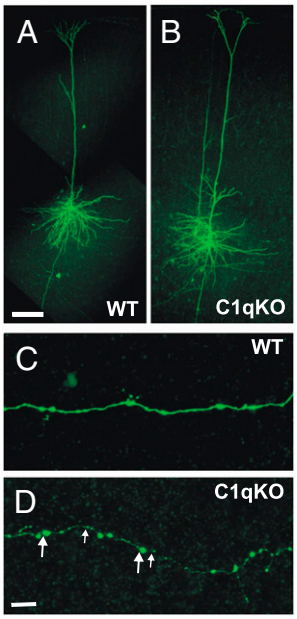

Fig. 3. Increased density of axonal boutons in cortical layer V pyramidal neurons of the C1q KO mice. (*A* and *B*) Confocal images of biocytin filled layer V pyramidal neurons of C1q KO (*A*) and WT (*B*) mice. (*C* and *D*) A segment of the axon from the control cell (*C*) and C1q KO neuron (*D*). Large and small arrows in *D* point to examples of large (>1 μm) and small (≤1 μm) boutons, respectively. (Scale bars: *A* for *A* and *B*, 100 μm; *D* for *C* and *D*, 10 μm.)

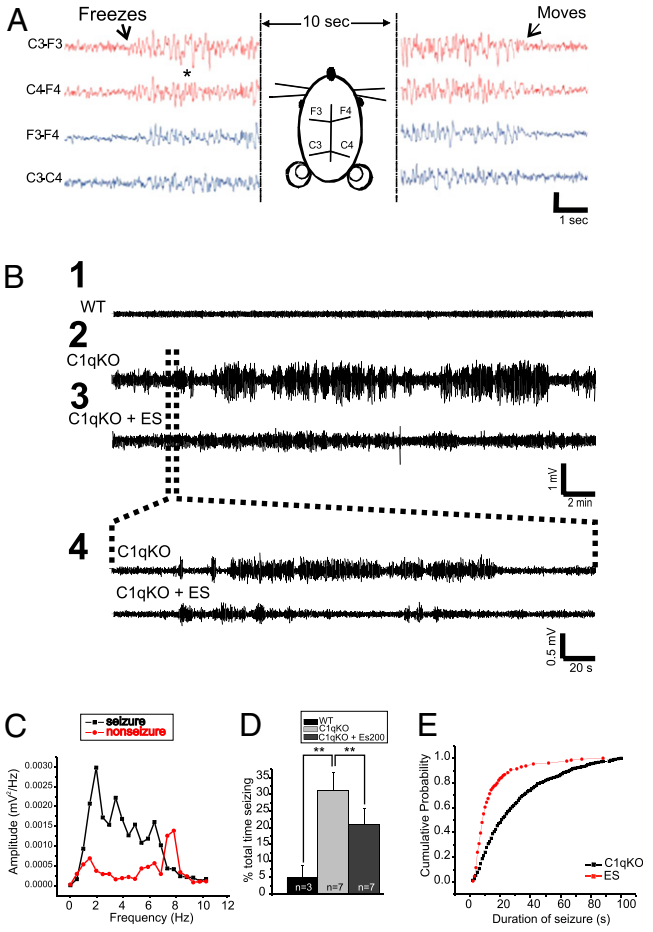

Fig. 4. C1q KO mice display spontaneous atypical absence seizures in EEG recordings. (*A*) Representative EEG trace of a seizure in a P27 C1q KO mouse. Arrows show beginning of behavioral arrest (freezing) at the onset of the seizure and return to normal exploratory behavior after the seizure ends. Horizontal diagram of mouse head shows placement of the four implanted epidural electrodes. (*B*) EEG recordings for 30 min from P31 WT (*B1*) and P30 C1q KO (*B2*) mice, both implanted at age P27, and from the same C1q KO mouse after i.p. injection with 200 mg/kg ethosuximide (*B3*). Brain waves from the C1q KO mouse show clear periods of seizures. Dotted lines show a blow-up view of a 5-min time trace (*B4*). (*C*) Graph depicts a Fourier transform power analysis of EEG frequencies during periods associated with spike activity. C1q KO recordings displayed seizure frequencies of 2–4 Hz, whereas WT recordings and background noise peaked at 7–8 Hz. (*D*) Total seizure time was significantly reduced with ethosuximide in C1q KO mice. Data were obtained by blind analysis of EEG data using amplitude criteria, accounting for activity in WT. (*E*) Cumulative probability plot of seizure duration measured in C1q KO mice before and after ethosuximide injection.

were occurring was further explored by chronically implanting epidural electrodes in 7 C1q KO and 3 WT mice (*Materials and Methods*) and simultaneously recording their video/EEGs. Surprisingly, C1q KO animals showed frequent seizures consisting of sudden behavioral arrest ("freezing" in place) with concurrent EEG paroxysms consisting of bihemispheric irregular EEG spike and slow wave activity lasting from 5 to 60 s (Fig. 4 *A* and *B 2* and *4*; see Movies S1 and S2 for video/EEG recordings). This activity differed from that described in genetic models of absence epilepsy (12) in that regular, rhythmic, well-formed spike-wave activity was not present. A Fourier transform power analysis revealed that EEGs during seizures had peak frequencies of 2–6 Hz, whereas background EEG activity in WT animals or activity between seizures in KO mice peaked at 7–8 Hz (Fig. 4*C*). Cross-correlation analysis of EEG activity during seizures showed synchrony between epileptiform events both from same-sided electrodes and between hemispheres (Fig. S4). The cross-correlograms between recorded bursts from four implanted electrodes showed a sharp peak around a lag time of 0 ms, indicating a high level of synchrony that was not detected by analysis of events between seizures. Focal or unilateral paroxysmal activity was not present in recordings lasting up to 1 h. Between these freezing episodes, C1q KOs showed normal exploratory behavior about the cage not different from that observed in WT mice. Implanted KO mice spent a significant amount of time in seizures (25–30%; Fig. 4*D*); however, WT mice had no similar EEG discharges and associated behavioral arrests (Fig. 4*B1*).

Identification of the sites of origin; distribution of electrographic abnormalities in other brain structures, for example, thalamocortical circuits; and classification of these seizures awaits results from additional experiments. However, the synchrony and bilateral nature of EEG abnormalities and the associated behavior resemble those of atypical absence seizures. For this reason we tested the effects of ethosuximide (ES) in the C1q KO mice, because this anticonvulsant is known to be effective in clinical absence seizures (13). The percent time in seizure activity was determined in 7 animals before and for 60 min after injection of 200 mg/kg i.p., a dose known to be effective in other models (13). Total time in seizure was significantly reduced by ES (Fig. 4*B3* and *4* and *D*). Cumulative probability plots (Fig. 4*E*) showed that ES significantly shortened seizure duration from a mean of 56.5 ± 6.9 s predrug to 26.7 ± 2.3 s after ES ($P < 0.05$), an effect lasting up to 30 min after a single injection. Although some prolonged seizure events lasting up to 60 s still occurred after ES, the majority of events lasted only 5–30 s (Fig. 4*E*).

Discussion

Failure To Prune as a Mechanism of Epilepsy. Here we show that in vitro neocortical slices from C1q KO, but not WT mice, generate spontaneous and evoked interictal epileptiform field potentials, and that implanted C1q KO mice have frequent atypical absence seizures. These results support the conclusion that there is enhanced excitatory synaptic connectivity in neocortex of these animals, which is likely the key factor leading to epileptogenesis. It is unlikely that the presence of bursts of EPSCs in the C1q KO slices contributed to the larger maps and increased hotspots, because we routinely added 10 μM APV in the recording ACSF to reduce slice excitability and eliminate polysynaptic responses, and we did not observe bursts of EPSCs in our mapping experiments. Thus, C1q KO mice represent a remarkable model of epilepsy associated with a genetically determined defect in the immune system and failure to prune excessive excitatory synaptic connections during development. Complete deficiency of C1q in humans is associated with immunological disorders; however, an epilepsy phenotype has not yet been noted in the few reported cases (14).

Formation of aberrant connections is regarded as a major contributing pathophysiological mechanism in a number of models of epileptogenesis (9); however, other structural-functional abnormalities such as decreases in GABAergic inhibition (15) and alterations in intrinsic neuronal properties (10) are present concurrently, so the role of hyperconnectivity alone as a mechanism of epileptogenesis has been difficult to assess. To the extent that the defect in C1q KO mice is limited to failure to prune excitatory synapses, this model provides an example of epilepsy due solely to enhanced connectivity. We cannot rule out the possibility that some, as yet undetected, additional abnormality contributes to chronic epileptiform activity in C1q KO cortex. C1q protein is expressed prominently at synapses in neocortex between P4 and 10 (6), so that pruning, or lack thereof, occurs in parallel with a number of other significant developmental changes that affect excitability in neocortex and, potentially, epileptogenesis (16).

We did not record from in vitro slices of C1q KO mice younger than P19, and our earliest implant was done at P18, so the devel-

opmental age for onset of epileptogenesis in vitro or in vivo in relation to the pruning defect is not clear. The importance of this question lies in the reported persistence of ordinarily eliminated connectivity when acute epileptiform activity is induced during a critical period for pruning (17) and the known role of activity in formation and refinement of connections (18). It is therefore possible that early epileptogenesis due to pruning failure, or other mechanisms, induces further increases in connectivity, so that the end result is determined by both genetic and activity-induced abnormalities. As noted above, a number of other genes are involved in the pruning process at different sites, so that later excitatory synapse elimination by proteins other than C1q, or a compensatory process such as sprouting of GABAergic axons and increased functional inhibition (19) could limit epileptiform activity at older ages.

Other Defects in Pruning. As noted above, the pruning process is influenced by a number of genes so that there may be other genetic or acquired abnormalities resulting in epileptogenesis due to failure to prune. For example, mutation of LGI1, a gene known to be involved in autosomal dominant lateral temporal lobe epilepsy (20), results in enhanced glutamatergic transmission in hippocampus in mice, due in part to decreased dendritic pruning and increased excitatory synapse formation during development (21). Although spontaneous seizures have not been observed in these mice, there is increased vulnerability to maneuvers that induce epileptiform activity in vivo and in vitro.

The seizures in C1q KOs are subtle and a similar behavioral phenotype resulting from other genetic pruning abnormalities could easily be overlooked. Immature callosal projections that are normally eliminated during development may become stabilized after epileptic cortical activity (17) and, paradoxically, blockade of activity during early development may result in a failure to eliminate recurrent excitatory connectivity in hippocampus (22). Lesions induced during critical developmental periods can also contribute to abnormalities in synapse elimination, and in some cases, to axon sprouting and enhanced dendritic arborizations (23). In the freeze lesion microgyral model, injury to the developing cortical plate at P1 causes profound changes in cortical connectivity that ultimately result in a focal epileptogenic neocortical malformation resembling human four-layered microgyria (24). Anatomical results suggest that the injury may result in persistence of abnormally distributed callosal connections (25). Both injury (26) and epileptiform activity (27) induce the release of trophic factors that may interfere with ontogenetic axonal pruning (27) and promote increased survival of aberrant connections.

Failure to prune may be an epileptogenic mechanism in other types of neocortical disorders including autism (28), fragile X syndrome, and other forms of genetic mental retardation (29). Pruning defects and aberrant neuritic sprouting have been documented in all of these disorders in both humans and animal models, and a significant fraction of patients with these diseases also have epileptic seizures.

Role of C1q Activation. Although C1q is developmentally downregulated (6), it is reactivated, along with other genes in the complement cascade after brain trauma (30), where it is part of a sustained inflammatory response to injury. It also been linked to the pathogenesis of Alzheimer's disease (31) and glaucoma (6). Long-lasting increases in C1q occur in microglia and some neurons in a rat model of temporal lobe epilepsy (TLE) after status epilepticus and in hippocampi of humans with TLE (32). An increase in C1q mRNA after kainate injection is blocked by barbiturates that prevent seizures and neurodegeneration (33). The recently described function of immune molecules in synaptic pruning in the retinogeniculate pathway (6) together with our results suggest that, in addition to a role in the inflammatory response, C1q activation may be involved in modifying axonal sprouting that is a consequence of injury and/or the excessive activity accompanying epileptiform discharges. Thus, the effects of activation of C1q or other molecules involved in pruning might either serve to balance excessive sprouting and retard epileptogenesis, or to eliminate newly formed synapses and adversely affect recovery from injury.

Materials and Methods

Slice Preparation and Field Potential Electrophysiology. All experiments were performed according to protocols approved by the Stanford Institutional Animal Care and Use Committee. Neocortical slices from 10 C1q KO and 6 WT mice (C56BL6 background) aged P19 (P0 = date of birth) to P30 were used for in vitro recordings. Animals were anesthetized with pentobarbital (55 mg/kg, i.p.) and decapitated, and the brains rapidly removed and placed in ice-cold (4 °C) oxygenated slicing solution containing 26 mM $NaHCO_3$, 2.5 mM KCl, 1.25 mM $NaH_2PO_4{\cdot}H_2O$, 10 mM $MgSO_4$, 0.5 mM $CaCl_2$, 11 mM D-glucose, and 234 mM sucrose. Coronal slices were cut with a vibratome (Leica VT1000S) through the sensorimotor cortex and maintained by using standard techniques. After ≈1 h incubation at 33 °C in artificial cerebrospinal fluid (ACSF), slices were held at room temperature. The ACSF contained 5 mM KCl, 10 mM D-glucose, 126 mM NaCl, 1.25 mM $NaH_2PO_4{\cdot}H_2O$, 1 mM $MgSO_4{\cdot}7H_2O$, 2 mM $CaCl_2{\cdot}2H_2O$; pH was titrated to 7.4 with NaOH.

For field potential recordings, slices (400 μm) were transferred to an interface chamber where they were perfused continuously (≈2.0 mL/min) with ACSF (33 °C) gassed with 95% O_2-5% CO_2. Sharp glass recording electrodes were pulled from borosilicate glass tubing (outer diameter, 1.5 mm), filled with 1 M NaCl (resistance of 5–10 MΩ), and placed in cortical layer V. Spontaneous activity was recorded for 5-m intervals and then stimuli consisting of single 50-μs current pulses were applied at increasing intensities (25-100 μA), via a bipolar stimulating electrode placed at the layer VI/white matter junction. A series of stimuli of increasing duration (threshold current for 50, 100, 200, and 400 μs) was then applied at 0.5 Hz. All responses were filtered at 4–5,600 Hz and recorded on a hard disk for later analysis.

Whole Cell Recordings and Laser Scanning Photostimulation of Caged Glutamate. Coronal cortical slices (350 μm) were prepared from P26–39 (P0 = the day of birth) C1q KO (C57BL6 background) and WT mice as above by using standard procedures. Slices were then incubated in ACSF at 32 °C for 1 h. The ACSF contained 126 mM NaCl, 2.5 mM KCl, 1.25 mM NaH_2PO_4, 2 mM $CaCl_2$, 2 mM $MgSO_4{\cdot}7H_2O$, 26 mM $NaHCO_3$, and 10 mM glucose (pH 7.4) when saturated with 95% O_2-5% CO_2. For whole cell recordings, each slice was perfused with recirculating ACSF containing 200 μM MNI-caged glutamate (4-methoxy-7-nitroindolinyl-caged L-glutamate, Tocris Bioscience) and 50 μM APV (Sigma) to block NMDA receptor components and polysynaptic events. An infrared video microscope (Axioskop; Zeiss) with a ×63, 0.9 numerical aperture water-immersion lens was used to visualize and target cortical layer V pyramidal neurons. Patch electrodes (3–5 MΩ resistance) were filled with a cesium based intracellular solution containing 125 mM Cesium methanesulfonate, 5 mM CsCl, 10 mM EGTA, 0.1 mM $CaCl_20.2H_2O$, 2 mM $MgCl_2O{\cdot}6H_2O$, 8 mM Hepes, 4 mM MgATP, 0.3 mM NaGTP, 5 mM QX314 and 0.5% biocytin. In current-clamp experiments, we used a K-gluconate-based intracellular solution containing 120 mM K-gluconate, 10 mM KCl, 11 mM EGTA, 1 mM $CaCl_2O{\cdot}2H_2O$, 2 mM $MgCl_2$, 10 mM Hepes, 0.5 mM NaGTP, 2 mM Na_2ATP and 0.5% biocytin. The osmolarity of the pipette solutions was adjusted to 285–295 mOsm and pH to 7.3 with 1 M KOH.

Glutamate uncaging was performed, whole cell voltage clamp recordings were made at −70 mV from layer V pyramidal neurons, and excitatory postsynaptic currents (EPSCs) were measured by using an Axon Instruments amplifier (Model 700B). Inhibitory postsynaptic currents (IPSCs) were recorded at +20 mV with a calculated E_{Cl} of −68 mV. Neurons were stimulated by a 300–800 μs UV laser flash (DPSS Lasers) through a ×5 UV objective. Positioning of the laser beam was precisely controlled with mirror galvanometers (model 6210; Cambridge Technology) under the control of scanning and data acquisition software. Each recording trace consisted of a 200-ms prestimulus baseline and an 800-ms poststimulus period. In most cases, two maps were recorded from each neuron and responses were averaged.

For each recording trace that corresponded to a photostimulation site, summation of the amplitude of all EPSCs detected within a time window between 8 and approximately 10 ms, and 100 ms postphotostimulation was used to generate a synaptic connectivity map. We defined "hotspots" as photostimulation sites from which one or more postsynaptic events could be evoked in the postphotostimulation time window. In each map, we calculated "region normalized" EPSC or IPSC amplitude by dividing the total amplitude of evoked events in a stimulus row by total number of spots in the same row. Hotspot ratio was calculated by dividing number of hotspots by the total number of spots in a stimulus row. The former was a comprehensive

measurement of intensity and range of connectivity in a map, whereas the latter was a measurement of the range of synaptic connectivity. For each neuron, an uncaging map was plotted by using the composite postsynaptic current amplitude within the detecting widow at every uncaging spot. In each group, a single average map of all mapped neurons was generated by mathematically aligning all maps to the location of somata, and dividing the summation of PSCs across all maps at each position by the total number of spots.

To determine whether the responses between the WT and KO were statistically significant, a two-way ANOVA was performed comparing the responses between the two groups and between different cortical depths. Further comparisons between control and C1q KO groups at each individual distance from the soma were made with a Student's *t* test.

Video/EEG Recordings in Vivo. Seven C1q KO (P18–27) and 3 WT (P24–30) mice were anesthetized with isofluorane and the skull exposed. Six silver wire electrodes (0.003-inch diameter; Medwire) insulated to within 0.5 mm of their cut ends were soldered to a microminiaturize connector. Dental cement was used to insulate the soldered contacts and fasten the connector to the skull at the midline. Two small holes were drilled in the skull just anterior to the bregma and the lambda and 2–3 mm from the midline on each side. The wire electrodes were inserted epidurally bilaterally through these holes. Two additional holes were made in the midline over frontal sinus and posterior to the lambda for reference and ground wire electrodes. Small pieces of Gelfoam were used to cover each hole, and dental cement was used to fasten electrodes to the skull. Animals were given carprofen 5 mg/kg s.c. postoperatively and allowed to recover for at least 3 d before recording. Simultaneous video/EEG recordings were obtained for each mouse for 1- to 2-h periods for up to 30 d after implantation, using a digital electroencephalograph (Xltek NeuroWorks). EEG signals were filtered through a 1-Hz high-pass filter and a 15-Hz low-pass filter, and converted to Clampfit 10.0 for analysis. Seizure activity was identified as high amplitude paroxysmal EEG discharges associated with episodes of abnormal behavior described below (Fig. 4*A* and Movies S1 and S2). To evaluate the effect of anticonvulsant drugs on spontaneous seizures in C1q KO mice, 7 animals were injected with ethosuximide (ES; 200 mg/kg, i.p.) and video/EEG recordings were made for 1 h after drug administration.

Data Acquisition and Analysis. ***In vitro slices.*** The incidence of epileptiform activity was measured in 1–5 slices from each mouse. Only slices in which stimuli evoked graded, short-latency field potentials of $\geq$0.5 mV in amplitude were used. Evoked epileptiform responses were identified as long-lasting (>150 ms), variable latency, polyphasic all-or-none events that followed the normal short latency field potential and often contained bursts of action potentials (e.g., Fig. 1*A*).

EEG analysis. Electrographic seizure durations were calculated from the video/EEG records of C1q KO and WT mice as the interval from the onset to the end of high amplitude, symmetrical EEG discharges accompanied by abnormal behavior (Fig. 4*A* and Movies S1 and S2). Seizure durations were also determined for the first 30 m after ES injections in C1q KO mice. Cumulative probability plots of seizure duration were calculated for C1q KO mice with and without ES injection, and a Kolmogorov-Smirnov test was used to determine statistical differences in median seizure duration. A Fourier transform power analysis using Clampfit 10.0 was used to determine the EEG frequency (hertz) during typical seizures and interictal periods. Statistical significance between control and C1q KO groups was determined with two-tailed Student's *t* test ($P < 0.05$). Data are presented as mean $\pm$ SEM. Microcal Origin 6.0 and Microsoft Excel software was used to perform all statistical analyses.

ACKNOWLEDGMENTS. This work was supported by NIH Grants NS12151 (to D.A.P.) and K99 NS057940 (to X.J.) and a Stanford University Undergraduate Research Grant (to Y.C.).

1. O'Leary DD, Stanfield BB (1986) A transient pyramidal tract projection from the visual cortex in the hamster and its removal by selective collateral elimination. *Brain Res* 392:87–99.
2. Killackey HP, Chalupa LM (1986) Ontogenetic change in the distribution of callosal projection neurons in the postcentral gyrus of the fetal rhesus monkey. *J Comp Neurol* 244:331–348.
3. Callaway EM, Katz LC (1990) Emergence and refinement of clustered horizontal connections in cat striate cortex. *J Neurosci* 10:1134–1153.
4. Low LK, Liu XB, Faulkner RL, Coble J, Cheng HJ (2008) Plexin signaling selectively regulates the stereotyped pruning of corticospinal axons from visual cortex. *Proc Natl Acad Sci USA* 105:8136–8141.
5. Huh GS, et al. (2000) Functional requirement for class I MHC in CNS development and plasticity. *Science* 290:2155–2159.
6. Stevens B, et al. (2007) The classical complement cascade mediates CNS synapse elimination. *Cell* 131:1164–1178.
7. Jin X, Prince DA, Huguenard JR (2006) Enhanced excitatory synaptic connectivity in layer v pyramidal neurons of chronically injured epileptogenic neocortex in rats. *J Neurosci* 26:4891–4900.
8. Tauck DL, Nadler JV (1985) Evidence of functional mossy fiber sprouting in hippocampal formation of kainic acid-treated rats. *J Neurosci* 5:1016–1022.
9. Salin P, Tseng GF, Hoffman S, Parada I, Prince DA (1995) Axonal sprouting in layer V pyramidal neurons of chronically injured cerebral cortex. *J Neurosci* 15:8234–8245.
10. Prince DA, Tseng GF (1993) Epileptogenesis in chronically injured cortex: in vitro studies. *J Neurophysiol* 69:1276–1291.
11. Dalva MB, Katz LC (1994) Rearrangements of synaptic connections in visual cortex revealed by laser photostimulation. *Science* 265:255–258.
12. Noebels J.L., Sidman R.L. (1979) Inherited epilepsy: spike-wave and focal motor seizures in the mutant mouse tottering. *Science* 204:1334–1336.
13. Patsalos PN (2005) Properties of antiepileptic drugs in the treatment of idiopathic generalized epilepsies. *Epilepsia* 46(Suppl 9):140–148.
14. Petry F, Loos M (2005) Common silent mutations in all types of hereditary complement C1q deficiencies. *Immunogenetics* 57:566–571.
15. Maglóczky Z, Freund TF (2005) Impaired and repaired inhibitory circuits in the epileptic human hippocampus. *Trends Neurosci* 28:334–340.
16. Avanzini G, de Curtis M, Pape HC, Spreafico R (1999) Intrinsic properties of reticular thalamic neurons relevant to genetically determined spike-wave generation. *Adv Neurol* 79:297–309.
17. Grigonis AM, Murphy EH (1994) The effects of epileptic cortical activity on the development of callosal projections. *Brain Res Dev Brain Res* 77:251–255.
18. Wiesel TN (1982) Postnatal development of the visual cortex and the influence of environment. *Nature* 299:583–591.
19. Bausch SB (2005) Axonal sprouting of GABAergic interneurons in temporal lobe epilepsy. *Epilepsy Behav* 7:390–400.
20. Zhou YD, et al. (2009) Arrested maturation of excitatory synapses in autosomal dominant lateral temporal lobe epilepsy. *Nat Med* 15:1208–1214.
21. Morante-Redolat JM, et al. (2002) Mutations in the LGI1/Epitempin gene on 10q24 cause autosomal dominant lateral temporal epilepsy. *Hum Mol Genet* 11:1119–1128.
22. Swann JW, Pierson MG, Smith KL, Lee CL (1999) Developmental neuroplasticity: roles in early life seizures and chronic epilepsy. *Adv Neurol* 79:203–216.
23. Marin-Padilla M (1997) Developmental neuropathology and impact of perinatal brain damage. II: white matter lesions of the neocortex. *J Neuropathol Exp Neurol* 56:219–235.
24. Jacobs KM, Gutnick MJ, Prince DA (1996) Hyperexcitability in a model of cortical maldevelopment. *Cereb Cortex* 6:514–523.
25. Rosen GD, Burstein D, Galaburda AM (2000) Changes in efferent and afferent connectivity in rats with induced cerebrocortical microgyria. *J Comp Neurol* 418: 423–440.
26. Nieto-Sampedro M, et al. (1982) Brain injury causes a time-dependent increase in neuronotrophic activity at the lesion site. *Science* 217:860–861.
27. Danzer SC, Crooks KR, Lo DC, McNamara JO (2002) Increased expression of brain-derived neurotrophic factor induces formation of basal dendrites and axonal branching in dentate granule cells in hippocampal explant cultures. *J Neurosci* 22: 9754–9763.
28. McCaffery P, Deutsch CK (2005) Macrocephaly and the control of brain growth in autistic disorders. *Prog Neurobiol* 77:38–56.
29. Comery TA, et al. (1997) Abnormal dendritic spines in fragile X knockout mice: Maturation and pruning deficits. *Proc Natl Acad Sci USA* 94:5401–5404.
30. Bellander BM, Singhrao SK, Ohlsson M, Mattsson P, Svensson M (2001) Complement activation in the human brain after traumatic head injury. *J Neurotrauma* 18: 1295–1311.
31. D'Andrea MR (2005) Evidence that immunoglobulin-positive neurons in Alzheimer's disease are dying via the classical antibody-dependent complement pathway. *Am J Alzheimers Dis Other Demen* 20:144–150.
32. Aronica E, et al. (2007) Complement activation in experimental and human temporal lobe epilepsy. *Neurobiol Dis* 26:497–511.
33. Rozovsky I, et al. (1994) Selective expression of clusterin (SGP-2) and complement C1qB and C4 during responses to neurotoxins in vivo and in vitro. *Neuroscience* 62: 741–758.